Radial slope measurement of dynamic transparent samples

2012 J. Opt. 14 045706

(http://iopscience.iop.org/2040-8986/14/4/045706)

J. Opt. **14** (2012) 045706 (7pp) doi:10.1088/2040-8978/14/4/045706

Radial slope measurement of dynamic transparent samples

David Ignacio Serrano-García[1], Noel-Ivan Toto-Arellano[1,2,3], Amalia Martínez-García[1] and Gustavo Rodríguez Zurita[3]

[1] Centro de Investigaciones en Óptica A. C., León, Guanajuato, México
[2] Universidad Tecnológica de Tulancingo, Tulancingo, Hidalgo, México
[3] Laboratorio de Óptica Física, Facultad de Ciencias Físico-Matemáticás de la Benemérita Universidad Autónoma de Puebla, Puebla, México

E-mail: david@cio.mx and ivantotoarellano@cio.mx

Received 20 October 2011, accepted for publication 21 February 2012
Published 16 March 2012
Online at stacks.iop.org/JOpt/14/045706

Abstract
An interferometric method to measure the radial slope of dynamic transparent samples is presented. We have implemented a simultaneous phase shifting Mach–Zehnder radial-shear interferometer (SPS-MZRI) using a phase grating to replicate the interference patterns and phase shifts modulated by polarization; the interferometer is capable of processing the optical phase data through the acquisition of *n*-interferograms captured simultaneously. The SPS-MZRI is capable of obtaining the radial phase derivative and associating it with its corresponding radial slope. The experimental results for static and dynamic samples are presented in this work, as well as the experimental evidence for the generation of spiral patterns.

Keywords: radial slope, phase shifting, interferometry, polarization

S Online supplementary data available from stacks.iop.org/JOpt/14/045706/mmedia

(Some figures may appear in colour only in the online journal)

1. Introduction

Several optical systems have been developed to retrieve optical phase data through the sequential acquisition of interferograms. Some improved systems achieve the simultaneous capture of several interferograms by means of polarization, such as through the use of micro-polarizer array elements [1], a point diffraction interferometer [2], a two-window phase grating interferometer [3], as well as through the use of a liquid-crystal spatial modulator [4], among others; these systems have been employed in several fields of application [5–8].

Obtaining the derivative of the wavefront object provides numerous advantages due to the high sensitivity that arises as a result of the abrupt phase changes [9]. In some cases, if the derivatives in the x and y directions are known, we can calculate the gradient information of the object, but this implies designing optical systems that generate shearing in both directions, or we may obtain shearing in each direction separately.

In several cases, radial symmetry is encountered, and it is strongly necessary to obtain the radial derivative of the incident wavefront in order to analyze the radial variations of the objects. For this reason, we propose the use of SPS-MZRI to obtain the radial derivative and its corresponding radial slope. Applications of radial-shear interferometers have been previously reported in optical testing [9, 10], aspherical surface measurement [11, 12], corneal topographic inspection [13, 14], adaptive optics [15], wavefront sensing [9, 16, 17] and beam characterization [18, 19], among others. Since many samples of interest to us have radial symmetry, we propose using a Mach–Zehnder radial-shear interferometer (MZRI), consisting of one telescope system on each arm.

The main purpose of this work is to measure variations in the radial slope of transparent objects by analyzing radial phase changes (previously reported for specular objects using ESPI and Shearography techniques [20]). Experimental results of temporal variations of evaporated oil placed on a slide using a tin soldering iron are presented. Additionally, a brief discussion is presented about the interference patterns

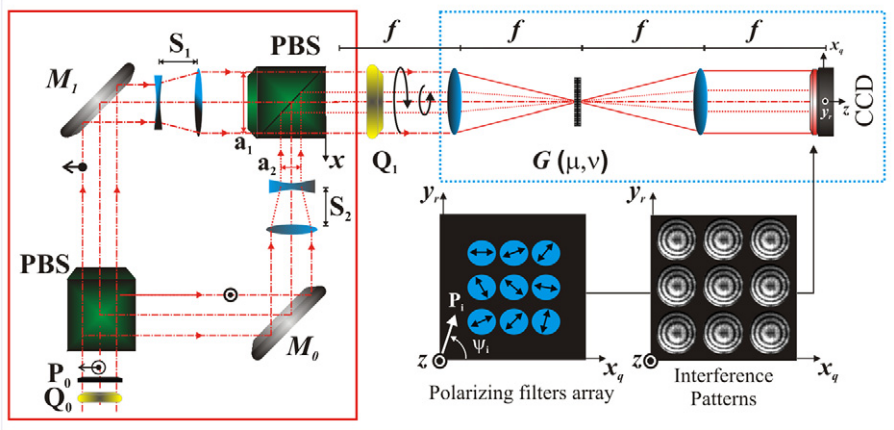

Figure 1. Optical setup. P_i: polarizers; Q_i: QWP operating at $\lambda = 632.8$ nm; PBS: polarizing beam splitter; M_i: mirrors; $G(\mu, \nu)$: phase grid. Order separation: F_0. Translation of coordinates around the order position: $x_q = x - qF_0$ and $y_r = y - rF_0$.

generation with spiral symmetry (spiralgrams) obtained with the optical system without the use of a Bessel beam.

2. Experimental setup

Figure 1 shows the experimental setup for radial slope measurements of transparent objects using a He–Ne laser operating at $\lambda = 632.8$ nm as a source. Polarized light at 45° enters the interferometer using a quarter-wave retarder plate Q_0 and a linear polarizer P_0. The Mach–Zehnder radial-shear interferometer (MZRI), shown within a rectangle, is composed of two telescope systems (S1, S2) [20], one in each arm, in order to generate two sheared beams with slightly different magnifications at the output of the interferometer and with crossed lineal polarization (vertical and horizontal, respectively). A wave retarder plate (QWP) of $\lambda/4$ (Q_1) is used to obtain cross circular polarization for each radial-shear wavefront (left and right, $\vec{J}_{\mathrm{L}}$ and $\vec{J}_{\mathrm{R}}$), which have equal amplitudes.

A 4-f system (dotted rectangle) is coupled at the end of the interferometer; this system consists of two similar achromatic lenses of focal length $f = 200$ mm and a phase grid $G(\mu, \nu)$ placed as the system's pupil, with a spatial period $d = 0.009090$ mm and its spacial frequency, by $\sigma = 1/d$. In the phase grid used, $\mu = u/\lambda f$ and $\nu = v/\lambda f$ are the frequency coordinates (u, v) scaled to wavelength λ and focal length f. A linearly polarized filter array is placed at the image plane, as shown in figure 1. Cross sections of the two sheared beams are $a_1 = 7.0$ mm and $a_2 = 8.6$ mm, and the relative magnification of the pupils is $M = 1.23$.

3. Polarizing phase shifting radial-shear interferometry

The polarized incident sheared beams with horizontal and vertical states can be written as:

$$O_1(x, y) = \frac{1}{\sqrt{2}}\begin{pmatrix}1\\0\end{pmatrix}\mathrm{circ}(r/M)\mathrm{e}^{\mathrm{i}\phi\left(\frac{x}{M},\frac{y}{M}\right)} \qquad \text{and}$$

$$O_2(x, y) = \frac{1}{\sqrt{2}}\begin{pmatrix}0\\1\end{pmatrix}\mathrm{circ}(r)\mathrm{e}^{\mathrm{i}\phi(x,y)}, \tag{1}$$

where $r = \sqrt{x^2 + y^2}$ and $M = 1/R$ define the relative magnifications of the pupils. At the output of the MZRI, a quarter-wave plate (QWP) is used with its fast axis at a 45° angle, yielding

$$\begin{aligned} O_1'(x, y) &= \frac{1}{\sqrt{2}}\begin{pmatrix}1\\\mathrm{i}\end{pmatrix}O_1(x, y)\\ O_2'(x, y) &= \frac{1}{\sqrt{2}}\begin{pmatrix}1\\-\mathrm{i}\end{pmatrix}O_2(x, y), \end{aligned} \tag{2}$$

which respectively represent left and right circularly polarized light. Then, the circular components, $O_1'(x, y)$ and $O_2'(x, y)$, go through an analyzer P_ψ, with its axis at an angle ψ represented by

$$P_\psi = \begin{pmatrix}\cos^2\psi & \cos\psi\sin\psi\\ \cos\psi\sin\psi & \sin^2\psi\end{pmatrix}.$$

The transmitted components are given by

$$\begin{aligned} O'(x, y)_{\mathrm{L}} &= P_\psi O_1'(x, y)\\ &= \frac{1}{\sqrt{2}}\begin{pmatrix}\cos\psi\\\sin\psi\end{pmatrix}\mathrm{e}^{\mathrm{i}[\phi\left(\frac{x}{M},\frac{y}{M}\right)+\psi]} \qquad \text{and}\\ O'(x, y)_{\mathrm{R}} &= P_\psi O_2'(x, y)\\ &= \frac{1}{\sqrt{2}}\begin{pmatrix}\cos\psi\\\sin\psi\end{pmatrix}\mathrm{e}^{\mathrm{i}[\phi(x,y)+\psi]}. \end{aligned} \tag{3}$$

The equations (3) represent linearly polarized beams with the same state of polarization. This allows the two components to interfere. These components have a phase difference, given by $\Delta\phi(x, y) = [\phi(x, y) - \phi(x/M, y/M)] - 2\psi$ [19–21]. As a result, and depending on the angle ψ, the analyzer P_ψ generates different phase shifts [22–25].

Considering equation (3), the interference pattern $I'(x, y)$ will be given by:

$$I'(x, y) = |[O'(x, y)_{\mathrm{L}} + O'(x, y)_{\mathrm{R}})]|^2, \tag{4}$$

where each sheared wavefront has circular polarization. The subscripts L and R represents left and right, respectively. In

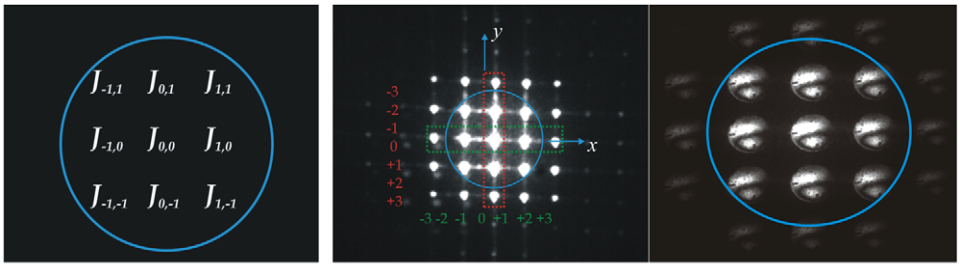

Figure 2. Interference pattern generated for the optical system convolved with the Fourier spectrum of the phase grating. (a) Bessel coefficients for each replica of the interference pattern. (b) Experimental diffraction orders. (c) Replicas of the interference pattern centered on each diffraction order.

this case, the interference pattern generated is given by:

$$I'(x, y) = 1 + \cos[2\psi - \Delta\phi(x, y)]. \tag{5}$$

Previous works have shown that when the interferometer is coupled to a 4-f system using phase grids or Bi-Ronchi gratings [9], it is possible to obtain replicas of the interference pattern, where each one of these replicas can be modulated by polarization.

4. Interference replicas generated by the phase grid

The coupled system uses a phase grid because of the great advantages involved, a major one being the use of a higher percentage of the incident energy than when using an absorption grating. The system uses two crossed phase gratings capable of obtaining up to 16 interference replicas with independent phase shifts that allow the use of the classical method of phase extraction [1–3].

The sinusoidal phase grid is generated by the multiplication of two sinusoidal phase gratings whose respective grating vectors are crossed. By considering the rulings of one grating along the μ direction, and the rulings of the second grating along the ν direction, the resulting phase grid can be written as

$$G(\mu, \upsilon) = \mathrm{e}^{\mathrm{i}2\pi A_\mathrm{g} \sin[2\pi X_0 \mu]} \mathrm{e}^{\mathrm{i}2\pi A_\mathrm{g} \sin[2\pi X_0 \upsilon]}$$
$$= \sum_{q=-\infty}^{\infty} J_q(2\pi A_\mathrm{g}) \mathrm{e}^{\mathrm{i}2\pi q X_0 \mu} \sum_{r=-\infty}^{\infty} J_r(2\pi A_\mathrm{g}) \mathrm{e}^{\mathrm{i}2\pi r X_0 \upsilon}. \tag{6}$$

The resulting Fourier transform of the centered phase grid can thus be written as

$$\tilde{G}(x, y) = \sum_{q=-\infty}^{q=\infty} \sum_{r=-\infty}^{r=\infty} J_q(2\pi A_\mathrm{g}) J_r(2\pi A_\mathrm{g}) \times \delta(x - qF_0, y - rF_0), \tag{7}$$

which consists of point-like diffraction orders distributed in the image plane, with $2\pi A_\mathrm{g}$ being the grating phase amplitude. The order separation is $F_0 \equiv \lambda f/d$, and $J_{q,r}$ denotes the Bessel function of the first kind and integer order q, r.

Thus, the interference patterns around a given order qr will have orthogonal circular polarization. To detect the irradiance over each replica of the interference pattern, centered around order qr, a linear polarized filter is placed at an angle $P(\psi)$ with respect to the horizontal axis. Only the contribution of one isolated term of order qr can be considered [3]. Then, the interference pattern $I_{q,r}(x, y)$ over the image plane of the system will be:

$$I_{q,r}(x, y) = \tilde{G}(x, y) \otimes I'(x, y), \tag{8}$$

where $\otimes$ denotes the convolution and the interference pattern $I'(x, y)$ and the diffraction grating defined by equation (7). Hence, the interference pattern at the image plane will be [21, 25]:

$$I_{q,r}(x, y) = \left[\sum_{q=-\infty}^{q=\infty} \sum_{r=-\infty}^{r=\infty} J_q(2\pi A_\mathrm{g}) J_r(2\pi A_\mathrm{g}) \delta(x - qF_0, y - rF_0) \right] \otimes [1 + \cos[2\psi - \Delta\phi(x, y)]]$$
$$= 2J_q^2 J_r^2 \{1 + \cos[2\psi - \Delta\phi(x_q, y_q)]\} \tag{9}$$

where $x_q = x - qF_0$ and $y_r = y - rF_0$ are the translation of coordinates around order position qr. The results are replicas of the main pattern with the intensity modulated by $J_{q,r}$ Bessel coefficients [3, 23, 24]. Figure 2 shows the experimental results obtained with the phase grid. The interference patterns that were used are enclosed in circles, with independent phase shifts that can be generated through the operation of linear polarizers. Figure 2(a) shows the overlapped diffraction orders, indicated by a subscript. Figure 2(b) shows the experimental 2D diffraction orders generated by the grid, where at least 16 diffraction orders with comparable intensities can be used. Figure 2(c) shows that each output intensity order is modulated by the diffraction orders of Bessel functions J_q and J_r, and that the image of the interference pattern generated by the MZRI is found centered on each of them.

The retardation error generated for the wave plates and the phase aberration of the diffractive elements can be neglected. However, the errors of the wave plates and polarizers, the intensity aberration of diffractive wavefronts and pixel mismatch should be corrected [26]. One should select good optical elements, high efficiency grating as well as adjust the optical setup carefully.

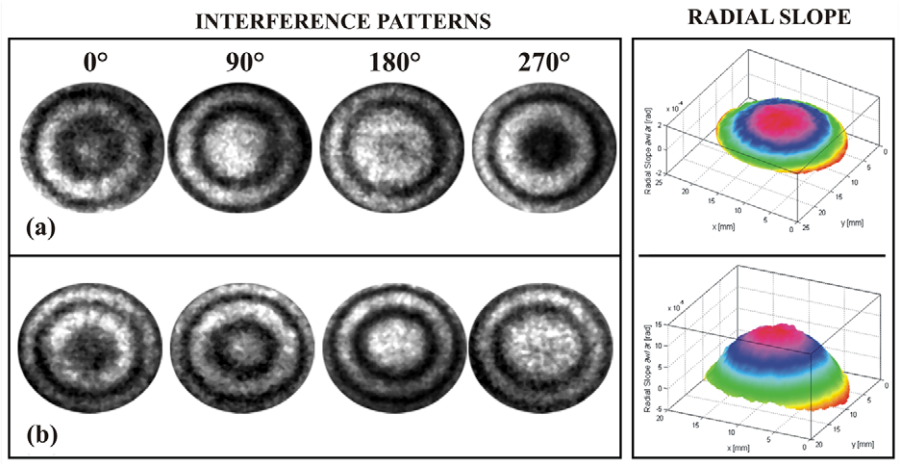

Figure 3. Several static test objects. (a) Reference wavefront. (b) Ophthalmic lens tested.

5. Radial slope of transparent samples

A transparent object also called a phase object can be represented, neglecting absorption, as:

$$O(x, y) = \mathrm{e}^{\mathrm{i}\phi(x,y)} \tag{10}$$

where $\phi(x, y)$ is a real function; this object is known as a phase object. To a thin phase object, it is considered that $|\phi(x, y)|^2 \ll 1$. In this case, the approximate equation used is [9]:

$$O(x, y) = 1 + \mathrm{i}\phi(x, y). \tag{11}$$

Since the system generates two images of the same object with different magnifications, the interference pattern obtained has radial symmetry [19, 21, 27, 28]. The interference pattern corresponds to concentric circular fringes. In this case, $r(x, y) = (x^2+y^2)^{1/2}$. From equation (11), the radial derivative is represented by

$$\frac{\partial O(r(x, y))}{\partial r(x, y)} = \mathrm{i}\frac{\partial \Delta\phi(x, y)}{\partial r(x, y)}. \tag{12}$$

The radial derivative of the phase object can be obtained through a small radial displacement Δr. Thus, we can approximate the radial change in phase with its radial derivative. The phase is obtained by using a four-step phase shifting algorithm [29, 30]

$$\frac{\partial \Delta\phi(x, y)}{\partial r(x, y)} = \tan^{-1}\left(\frac{I_1(x, y) - I_3(x, y)}{I_2(x, y) - I_4(x, y)}\right). \tag{13}$$

The intensity measurements, I_i, are captured in a single shot, with the different values of ψ given by $\psi_1 = 0$, $\psi_2 = 45$, $\psi_3 = 90$, $\psi_4 = 135$. The phase change introduced due to out-of-plane (w) deformation is given by [31, 32]:

$$\frac{\partial\phi(x, y)}{\partial r(x, y)} = \frac{4\pi}{\lambda}\frac{\partial w(r(x, y))}{\partial r(x, y)}\Delta r. \tag{14}$$

The fringe pattern obtained corresponds to contours of $\partial w(r)/\partial r$. The change in the phase object associated with the radial slope is [33, 34]:

$$\frac{\partial w(r(x, y))}{\partial r(x, y)} = C_0\frac{\partial O(x, y)}{\partial r(x, y)}, \tag{15}$$

with $c_0 = \lambda/4\pi\Delta r$. It can be noticed that the radial derivative of the phase object is proportional to the out-of-plane (w) deformation [34]. Also, there exists a constant phase relationship of $\pi/2$ due to the term $i = \mathrm{e}^{\mathrm{i}\pi/2}$.

6. Experimental results

The optical system implemented to obtain the radial slope of transparent objects is shown in figure 1. The phase gratings used are nominally identical. According to the manufacturer, the grating features are: frequency of $\sigma = 110$ lines mm^{-1}, dimension of 25 × 25 mm^2, dimensional tolerance of ±0.5 mm and a substrate of optical crown glass. The monochromatic camera (CMOS) used in the image capture has 1280 pixels × 1024 pixels. Four interference patterns were captured simultaneously. Each pattern was filtered using a conventional low-pass filter to remove sharp edges and details. Every interferogram used was subjected to a rescaling and normalization process [35] to reduce differences of irradiance and fringe modulation. This procedure generates patterns of equal intensities and equal fringe modulation. In order to obtain the optical phase, a reference phase map is first taken, to be then subtracted from the phase map of the phase object in each capture.

Figure 3 shows experimental results for samples with radial symmetry and their associated radial slopes. Figure 3(a) presents a characteristic radial-shear interference pattern obtained by interfering spherical wavefronts as a reference. The interference patterns obtained represent contours of constant $r(\partial w/\partial r)$, being symmetric about the center of curvature of the incident wavefront. Figure 3(b) shows the radial slope of an ophthalmic lens presenting a cross section of 5 mm, to show the variation with respect to the slope in figure 3(a).

Figure 4 shows the deformation caused by gravity in a lubricating oil drop placed over a microscope slide. The

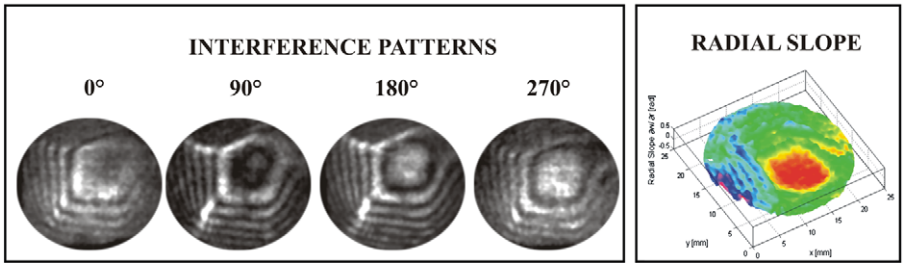

Figure 4. Lubrication oil over a microscope slide.

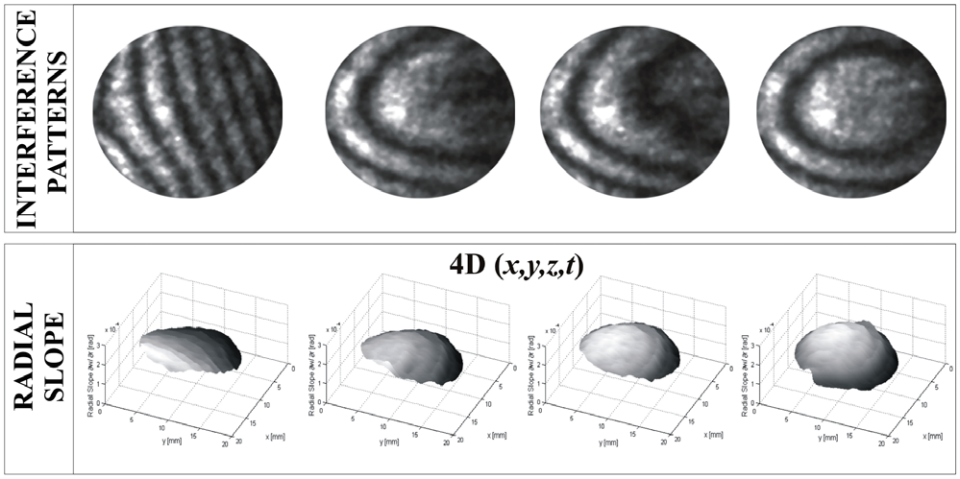

Figure 5. Dynamic distributions of radial slope are presented in 4D (representative frames). Upper row: interference patterns (Media 1 available at stacks.iop.org/JOpt/14/045706/mmedia). Lower row: evolution of radial slope (Media 2 available at stacks.iop.org/JOpt/14/045706/mmedia). Animation:14 captures per second.

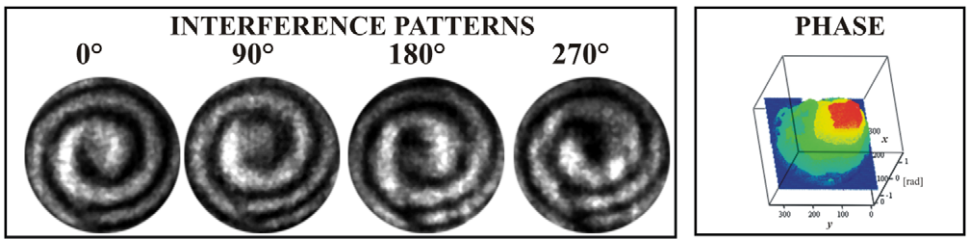

Figure 6. Experimental spiralgrams and phase recovery.

fringe pattern represents the stress field associated with the stabilization of the oil drop on the slide. This variation can be observed due to radial slope variation. A low contrast is observed in some fringe pattern sections, due to the high density oil layer, hence losing the thin phase objects condition.

With the purpose of showing the capability of the optical system to study dynamic events (4D), we present results for lubricating oil that was placed on a microscope slide and then evaporated using a tin soldiering iron. The corresponding interferograms for successive captures of the CCD camera are shown in figure 5 (upper row, Media 1 available at stacks.iop.org/JOpt/14/045706/mmedia), along with its associated radial slope (lower row, Media 2 available at stacks.iop.org/JOpt/14/045706/mmedia). It is important to mention that the results are obtained using an optical table without pneumatic suspension, and that the polarized array used is formed by conventional polarized film placed at different angles, with the advantage of not using a micro-polarized array.

7. Spiralgrams

To show some advantages of the optical system implemented, an alternative method to obtain spiralgrams without using Bessel beams is presented. Figure 6 shows preliminary results of a spiral pattern (spiralgram) obtained through the use of the radial symmetry of the MZRI. The spiralgram was obtained when it introduced a phase change of $\pi/2$ in the half of the wavefront in one arm of the MZRI. This generated a phase dislocation, resulting in a similar effect of a spiral phase plate or a phase hologram [36].

The experimental results show a simple method to generate spiral beams, or spiralgram which are useful in the determination of the sign of the phase when it is used in simultaneous phase shifting interferometry. The same results and symmetries can be obtained by truncating a Bessel beam generated by an axicon or an annular slit. However, the proposed method here simplifies the arrangement, since it does not require the manufacturing of special optical components. Thereby, under some conditions, the application of this technique can also be used for singular optics. Additionally, the conventional demodulation procedures for phase calculations were performed using solutions for the *n*-symmetrical four-step algorithms. Due to this, we can apply the techniques of simultaneous phase shift. The proposed method can be extended to apply it to the analysis of dynamic phase objects.

8. Conclusions

We have demonstrated the use of an SPI-MZRI to simultaneously achieve several shearograms for slope measurements using phase shifting techniques. We present experimental results to study static and dynamic objects by using a radial-shear interferometer. The advantage of these systems is that the radial slope of the phase object is obtained. The experimental evidence for the generation of spiralgrams illustrates additional advantages of the optical system.

Acknowledgments

The authors thank M A Ruiz for his contribution in proofreading the manuscript. Enlightening comments and references from anonymous referees are also acknowledged. The experimental results are part of the bilateral projects between Mexico–Chile (CONACYT–CONICYT) and Mexico–Italy (CONACYT–MAE).

D-I Serrano-García (grant 227470/31458) is very grateful to CONACYT for the graduate scholarship granted, and expresses sincere appreciation to Geliztle.

N-I Toto-Arellano expresses sincere thanks to Luisa, Miguel and Damian for the support provided, and to Sistema Nacional de Investigadores (SNI) for grant 47446. Partial support from CONACYT and Vicerrectoría de Investigación y Estudios de Posgrado (VIEP) through projects 124145 and 154984 is also acknowledged.

References

[1] Novak M, Millerd J, Brock N, North-Morris M, Hayes J and Wyant J C 2005 Analysis of a micropolarizer array-based simultaneous phase-shifting interferometer *Appl. Opt.* **44** 6861–8

[2] Neal R M and Wyant J C 2006 Polarization phase-shifting point-diffraction interferometer *Appl. Opt.* **45** 3463–76

[3] Rodriguez-Zurita G, Toto-Arellano N I, Meneses-Fabian C and Vázquez-Castillo J F 2008 One-shot phase-shifting interferometry: five, seven, and nine interferograms *Opt. Lett.* **33** 2788–90

[4] Baker K L and Stappaerts E A 2006 A single-shot pixellated phase-shifting interferometer utilizing a liquid-crystal spatial light modulator *Opt. Lett.* **31** 733–5

[5] Wyant J C 2004 Vibration insensitive interferometric optical testing *Frontiers in Optics, OSA Technical Digest* (Optical Society of America) OTuB2

[6] Araiza-Esquivel M A, Martínez-León L, Javidi B, Andrés A, Lancis J and Tajahuerce E 2011 Single-shot color digital holography based on the fractional Talbot effect *Appl. Opt.* **50** B96–B101

[7] Nomura T, Murata S, Nitanai E and Numata T 2006 Phase-shifting digital holography with a phase difference between orthogonal polarizations *Appl. Opt.* **45** 4873–7

[8] Chen L C, Yeh S L, Tapilouw A M and Chang J C 2010 3-D surface profilometry using simultaneous phase-shifting interferometry *Opt. Commun.* **283** 3376–82

[9] Toto-Arellano N I, Martínez-García A, Rodríguez-Zurita G, Rayas-Álvarez J A and Montes-Perez A 2010 Slope measurement of a phase object using a polarizing phase-shifting high-frequency Ronchi grating interferometer *Appl. Opt.* **49** 6402–8

[10] Steel W H 1965 A radial shear interferometer for testing microscope objectives *J. Sci. Instrum.* **42** 102–4

[11] Hariharan P, Oreb B F and Wanzhi Z 1984 Measurement of aspheric surfaces using a microcomputer controlled digital radial-shear interferometer *J. Mod. Opt.* **31** 989–99

[12] Liu D, Yang Y, Shen Y, Weng J and Zhuo Y 2007 System optimization of radial shearing interferometer for aspheric testing *Proc. SPIE* **6834** 68340U

[13] Kowalik W W, Garncarz B E and Kasprzak H T 2002 Corneal topography measurement by means of radial shearing interference: part I—theoretical considerations *Optik* **113** 39–45

[14] Kowalik W W, Garncarz B E and Kasprzak H T 2003 Corneal topography measurement by means of radial shearing interference: part III—measurements errors *Optik* **114** 199–206

[15] Shirai T, Barnes T H and Haskell T G 2001 Real-time restoration of a blurred image with a liquid-crystal adaptive optics system based on all-optical feedback interferometry *Opt. Commun.* **118** 275–82

[16] Geary J M 2000 Wavefront sensors *Adaptive Optics Engineering Handbook* ed R K Tyson (Boca Raton, FL: CRC Press) chapter V, pp 123–50

[17] Hutchin R A 1985 Combined shearing interferometer and Hartmann wavefront sensor *Patent Number* 4518854

[18] Hernandez-Gomez C, Collier J L, Hawkes S J, Danson N, Edwards C B, Pepler D A, Ross I N and Winstone T B 2000 Wave-front control of a large-aperture laser system by use of a static phase corrector *Appl. Opt.* **39** 1954–61

[19] Liu D, Yang Y, Wang L and Zhuo Y 2007 Real-time diagnosis of transient pulse laser with high repetition by radial shearing interferometer *Appl. Opt.* **46** 8305–14

[20] Ganesan A R, Sharma D K and Kothiyal M P 1988 Universal digital speckle shearing interferometer *Appl. Opt.* **27** 4731–4

[21] Lago E L and de la Fuente R 2008 Amplitude and phase reconstruction by radial shearing interferometry *Appl. Opt.* **47** 372–6

[22] Toto-Arellano N-I *et al* 2011 *J. Opt.* **13** 115502

[23] Rodríguez-Zurita G *et al* 2009 Adjustable lateral-shear single-shot phase-shifting interferometry for moving phase distributions *Meas. Sci. Technol.* **20** 115902

[24] Toto-Arellano N I, Rodriguez-Zurita G, Meneses-Fabian C and Vázquez-Castillo J 2008 Phase shifts in the Fourier spectra of phase gratings and phase grids: an application for one-shot phase-shifting interferometry *Opt. Express* **16** 19330–41

[25] Serrano-García D I, Toto-Arellano N-I, Martínez García A, Rayas Álvarez J A, Téllez-Quiñones A and Rodríguez-Zurita G 2011 Simultaneous phase-shifting cyclic interferometer for generation of lateral and radial shear *Rev. Mex. Fís.* **57** 255–8

[26] Kemao Q, Xiaoping W and Asundi A 2002 Grating-based real-time polarization phase-shifting interferometry: error analysis *Appl. Opt.* **41** 2448–53

[27] Hariharan P and Sen D 1961 Radial shearing interferometer *J. Sci. Instrum.* **38** 428–32

[28] Malacara D 1974 Mathematical interpretation of radial shearing interferometers *Appl. Opt.* **13** 1781–4

[29] Barrientos-García B, Moore A J, Pérez-López C, Wang L and Tschudi T 1999 Spatial phase-stepped interferometry using a holographic optical element *Opt. Eng.* **38** 2069–74

[30] Malacara D, Servin M and Malacara Z 2005 Phase detection algorithms *Interferogram Analysis for Optical Testing* (New York: Wiley) chapter 6

[31] Sirohi R S 1984 Speckle shearing interferometry *Opt. Laser Technol.* **16** 251–4

[32] Rastogi P K 1996 Measurement of in-plane strains using electronic speckle and electronic speckle-shearing pattern interferometry *J. Mod. Opt.* **43** 1577–81

[33] Ng T W 1995 Digital speckle pattern interferometer for combined measurements of out-of-plane displacement and slope *Opt. Commun.* **116** 31–5

[34] Bhaduri B, Mohan N K and Kothiyal M P 2006 A dual-function ESPI system for the measurement of out-of-plane displacement and slope *Opt. Lasers Eng.* **44** 637–44

[35] Quiroga J A, Gómez-Pedrero J A and García-Botella A 2001 Algorithm for fringe pattern normalization *Opt. Commun.* **197** 43–51

[36] Rodríguez-Zurita G, Toto-Arellano N I, Arroyo-Carrasco M L, Meneses-Fabián C and Castillo J F V 2009 Experimental observation of spiral patterns by obstruction of Bessel beams: application of single shot phase-shifting interferometry *Conf. on Lasers and Electro-Optics/Pacific Rim 2009* (Optical Society of America) ThE1_4